Combined 6,7Li NMR and molecular dynamics study of Li diffusion in Li2TiO3

ARTICLE *in* THE JOURNAL OF PHYSICAL CHEMISTRY C · NOVEMBER 2009

Impact Factor: 4.77 · DOI: 10.1021/jp9072125

Combined ^{6,7}Li NMR and Molecular Dynamics Study of Li Diffusion in Li_2TiO_3

M. Vijayakumar, Sebastien Kerisit, Zhenguo Yang, Gordon L. Graff, Jun Liu, Jesse A. Sears, Sarah D. Burton, Kevin M. Rosso,* and Jianzhi Hu*

Pacific Northwest National Laboratory, Richland, Washington 99352

Received: July 28, 2009; Revised Manuscript Received: September 15, 2009

Understanding lithium diffusion properties in electrode materials is important for designing rechargeable lithium-ion batteries with improved performance. In this work, the lithium dynamics in layered Li_2TiO_3 were characterized using a combination of ^{6,7}Li nuclear magnetic resonance (NMR) over a wide temperature range (150−500 K) and molecular dynamics (MD) simulations. The ^{7}Li static NMR and stimulated echo experiments show slow and partial lithium diffusion in Li_2TiO_3. The high-field (21.1 T) ^{6}Li magic-angle spinning NMR shows a new tetrahedral lithium site along with the three crystallographic octahedral sites in Li_2TiO_3 sample. MD simulations predict that lithium can occupy a tetrahedral site if two or more vacancies exist in the vicinity, which may result, for example, from the presence of a Ti defect in the $LiTi_2$ layer. ^{6}Li two-dimensional (2D) exchange NMR experiments show evidence of lithium diffusion between the pure Li and $LiTi_2$ layers along the *c* axis. Although the 2D exchange NMR data are not sensitive to lithium diffusion in the *ab* plane, MD simulations show that lithium diffusion in the pure Li layer is equally probable. Combining these results, a detailed picture of the lithium diffusion pathways in Li_2TiO_3 is presented.

Introduction

Lithium metatitanate (Li_2TiO_3) is a technologically important material with many applications. For example, it has been used as an electrode material in lithium-ion batteries,[1,2] as a double layer cathode material in molten carbonate fuel cells,[3] and as a solid breeder material in the blanket of fusion reactors.[4] In the field of lithium-ion batteries, Li_2TiO_3 has been reported to be capable of stabilizing the structure of high-capacity cathode materials such as $LiFeO_2$, $LiMnO_2$, $LiCrO_2$, and $LiNiO_2$.[5−8] The layered solid solutions, with formulas $xLiMO_2 - (1 - x)Li_2TiO_3$ (M = Fe, Mn, Cr, Ni), lead to promising cathode materials, which provide higher Coulombic efficiencies on extended cycling between 4.6 and 2.3 V.[1,6] When used as a breeder material, Li_2TiO_3 produces tritium atoms by lithium transmutation and transports the heat generated by the nuclear reaction to the coolant.[9] Because of its many important applications, the mechanical and thermal properties of Li_2TiO_3 have been extensively investigated.[10−12] The electrical and thermal conductivity of Li_2TiO_3 has also been probed using traditional impedance measurements.[13,14] It has been reported that Li_2TiO_3 shows poor electrical conductivity, that is, on the order of 10^{-7} S cm^{-1} at 400 K.[13] Despite all of the prior investigations, the detailed diffusion pathways of lithium in the bulk and the occupancy of lithium in the lattice as well as the effects of the defects that are critically important for understanding the poor electrical conductivity of Li_2TiO_3 materials are not known. This is largely because the impedance measurements only probe the overall conductivity, which is a combination of lithium diffusion and electronic contributions. In particular, in conductivity measurements, the intrinsic properties of the material of interest are sometimes masked by those of grain boundaries or impurities. Therefore, a better analytical tool is needed for identifying the detailed lithium diffusion properties of Li_2TiO_3.

Nuclear magnetic resonance (NMR) is nucleus specific (i.e., only the local environment of the particular nucleus under study is probed by NMR), nondestructive, and stringently quantitative, and therefore can offer valuable information about diffusion processes in ion conducting materials. Indeed, details in local structure and dynamics of lithium-ion conducting materials have been unraveled with solid-state NMR.[15] Although NMR can offer a conspicuous view of the diffusion properties of complex materials, interpretation of NMR data is theoretically complex and thus often relies on complementary information from computational models to elucidate the ion dynamics and diffusion pathways. One example of choice is the use of potential-based molecular dynamics (MD) simulations, which offer several advantages. First, it allows one to perform dynamical simulations of lithium diffusion for long periods of time. This makes the direct calculation of lithium diffusion coefficients and diffusion pathways possible and allows for directly identifying any mixing between different lithium sites. Second, it allows one to treat much larger lattices than used with first-principles techniques, which, in turn, allows one to consider a wide range of conditions from the infinite dilution limit to high lithium contents with small concentration intervals. Therefore, by combining information obtained from NMR and MD simulations, we can draw a prominent picture of the diffusion processes in ion conducting materials.

In this Article, we present results from solid-state ^{6,7}Li NMR and computational studies of the lithium local structure and diffusion processes in Li_2TiO_3. The lithium dynamics are analyzed with powerful NMR methods such as traditional relaxation NMR,[16] two-dimensional (2D) exchange NMR,[17] and newly established quadrupolar spin-alignment echo (SAE) technique.[18] The lithium local structure and probable diffusion pathways are computed using potential-based molecular dynamics simulations. These results constitute a first step toward understanding the lithium local diffusion mechanisms in lithium metatitanate and will provide a basis for further investigations of lithium diffusion in layered cathode materials.

* Corresponding authors. J.H.: phone, (509) 371-6544; fax, (509) 371-6546; e-mail, jianzhi.hu@pnl.gov. K.M.R.: phone, (509) 371-6357; e-mail, kevin.rosso@pnl.gov.

10.1021/jp9072125 CCC: $40.75
Published on Web 10/27/2009

Experimental Section

The monoclinic Li_2TiO_3 sample was prepared by using a simple and low cost hydrothermal treatment method.[19] LiOH (Aldrich) and nanosized anatase TiO_2 (Aldrich) were used as starting materials with the amounts of LiOH and TiO_2 chosen to achieve a Li/Ti ratio of 2. The anatase TiO_2 and LiOH were dissolved in 20 mL of deionized water and stirred at room temperature for 6 h and then heat treated in a Teflon coated autoclave vessel at 180 °C for 12 h to facilitate the hydrothermal reaction. Next, the products were filtered and rinsed with copious amount of water and heat treated at 500 °C for 2 h under nitrogen atmosphere. The products were identified by X-ray powder diffractometry (XRD) using a Philips Xpert X-ray diffractometer using Cu Kα radiation at $\lambda \approx 1.54$ Å. The resulting XRD patterns were compared to standard power diffraction data (JCPDS#33-0831) and revealed that the final product was pure monoclinic Li_2TiO_3.

^{7}Li static NMR measurements were performed using a Chemagnetics 300 spectrometer ($B_0 = 7.05$ T, and ^{7}Li Larmor frequency of 116.53 MHz). The microscopic Li jump rates were measured by recording two-time ^{7}Li NMR spin-alignment echoes (SAEs). The ^{7}Li NMR spin-alignment echoes experiment is based on the three-pulse sequence introduced by Jeener and Broekaert ($90°-t_p-45°-t_m-45°-$acq).[20] The pulse sequence and phase cycling are used as reported by Böhmer et al.[21,22] A short preparation time ($t_p = 15$ μs) is used to ensure that the preferential spin-alignment order is created after the first 45° pulse, and various mixing times (t_m) ranging from 10^{-6} to 100 s were used before final readout pulse. The short preparation time ($t_p = 15$ μs) is chosen so that the echo signal mainly arises from quadrupolar interactions and the homo- and heteronuclear contributions to the echo will be very small.[23] Extensive phase cycling was used to pick out the correct coherence pathway, and final echoes were read out at $t = t_p$, where t is the acquisition time. Up to 128 signals were accumulated for each stimulated echo. The 90° pulse length was about 2.5 μs and guaranteed a nonselective excitation of the entire ^{7}Li spin-alignment spectrum.

^{6}Li NMR measurements were performed on a Varian 900 Inova magnet ($B_0 = 21.1$ T and ^{6}Li Larmor frequency of 113.56 MHz) with magic-angle spinning (MAS) at 7 kHz using 5 mm zirconia rotors and a custom-made high-temperature MAS probe. Chemical shifts were externally referenced to a 1 M LiCl solution ($\delta_{iso} = 0$ ppm). The estimated uncertainty in chemical shifts was 0.1 ppm and was determined through calibration using the same reference sample. Accurate intensities of the contributions in each spectra were obtained from fitting the line shapes of the resonance lines with a mix of Gaussian and Lorentzian line-shapes using the DMFIT program.[24] Two-dimensional exchange spectra were acquired using a three-pulse sequence[25] with mixing times of 500 μs and 1 s. The number of slices in the indirect dimension was 48 with 32 transients averaged per slice. The 16-step phase cycling with hyper complex data acquisition mode was used in both spectra. The lithium metatitanate sample was heat treated at 100 °C for 2 h before packing in NMR rotors to remove any surface-adsorbed water.

Computational Methods

Potential Model. The calculations reported in this work are based on the Born model of solids,[26] in which the atoms of a system are represented as point-charge particles that interact via long-range Coulombic forces and short-range interactions. The latter are described by parametrized functions and represent the repulsion between electron-charge clouds and the van der Waals attraction forces. In this work, the short-range interactions are described using a Buckingham potential, and therefore the pairwise interaction energy takes the following form:

$$U_{ij} = \frac{1}{4\pi\varepsilon_0}\frac{q_i q_j}{r_{ij}} + A_{ij}\exp\left(-\frac{r_{ij}}{\rho_{ij}}\right) - \frac{C_{ij}}{r_{ij}^6} \qquad (1)$$

The parameters (q, A, ρ, and C) used in this study are those optimized by Matsui and Akaogi (MA)[27] for the TiO_2 polymorphs rutile, anatase, brookite, and TiO_2-II. In a previous publication,[28] we derived a shell model version of the MA potential that allows for modeling electron small polarons in these materials and gives excellent agreement with the reorganization energies obtained from density functional theory calculations[29] of several polaron transfers in titania polymorphs. A full description of the approach taken to derive these potential parameters is given in that publication.[28] In the shell model,[30] a polarizable ion is composed of two particles, a core and a shell, which share the ion's charge and are linked by a harmonic spring, k:

$$U_{c-s} = k \times r_{c-s}^2 \qquad (2)$$

where r_{c-s} is the core−shell separation distance. The potential parameters used to describe lithium ions were determined by fitting the potential parameters for Li to the lattice parameters, lattice constants, and bulk modulus of Li_2O while keeping the MA potential parameters constant. The lithium partial charge was determined from the Li_2O stoichiometry while keeping the oxygen partial charge from the MA model constant (i.e., $q_{Li} = -q_O/2 = +0.549$ e). Details of the derivation of the Li parameters and their performance will be provided in a future publication. All of the potential parameters used in this work are summarized in Table 1.

TABLE 1: Potential Parameters Used in This Work[a]

Core and Shell Charges[b]		
species	core (e)	shell (e)
Ti^{4+}	2.196	
Ti^{3+}	1.647	
Li^+	0.549	
O^{2-}	0.500	−1.598000

Buckingham Potential Parameters[c]			
ion pair (ij)	A_{ij} (eV)	ρ_{ij} (Å)	C_{ij} (eV Å^6)
Li−Li	38 533.955	0.100	0.00
Ti−Li	33 089.570	0.127	0.00
Ti−Ti	31 120.528	0.154	5.25
Ti−O	16 957.710	0.194	12.59
Li−O	15 465.549	0.167	0.00
O−O	11 782.884	0.234	30.22

[a] The oxygen core−shell spring constant, k, is set to 44.3 eV Å^{-2}. [b] Core−shell interaction potential form: $V = k \times r_{c-s}^2$. [c] Buckingham potential form: $V_{ij} = A_{ij} \times \exp(-r_{ij}/\rho_{ij}) - C_{ij}r_{ij}^{-6}$.

The ability of the potential model for simulating Li_2TiO_3 was evaluated by comparing the calculated and experimental lattice parameters. A constant-pressure energy minimization (i.e., zero Kelvin) of the Li_2TiO_3 unit cell with the computer program METADISE[31] yielded $a = 5.068$ Å, $b = 8.796$ Å, $c = 9.509$ Å, and $\beta = 100.242°$. A 200 ps NPT molecular dynamics simulation at 300 K with the computer program DL_POLY[32] resulted in a slight thermal expansion with $a = 5.100$ Å, $b =$

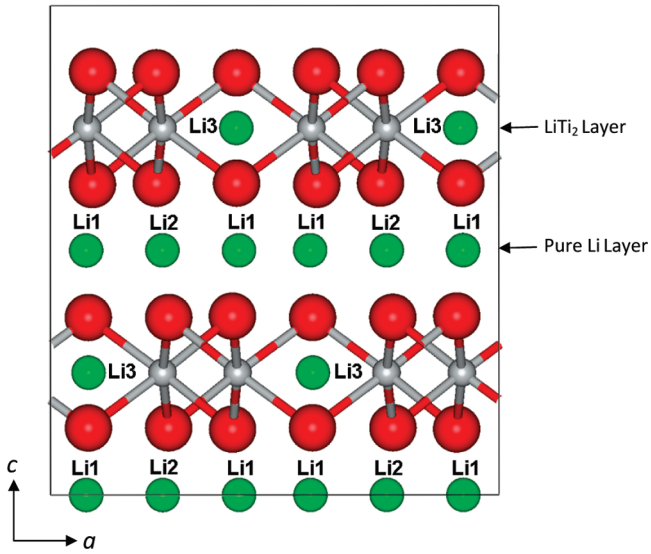

Figure 1. The crystal structure of monoclinic Li_2TiO_3, (space group $C2/c$) viewed along the b axis showing the three Li crystallographic sites (as reported in ref 34). The pure Li layer and $LiTi_2$ layer are arranged alternatively along the c axis. Lithium atoms are shown in green, oxygen atoms in red, and titanium atoms in gray.

8.852 Å, $c = 9.660$ Å, and $\beta = 100.234°$. In 1969, Dorrian and Newnham[33] published the following lattice parameters: $a = 5.041$ Å, $b = 8.806$ Å, $c = 9.726$ Å, and $\beta = 100.01°$. More recently, the single-crystal X-ray diffraction (XRD) data of Kataoka et al.[34] yielded $a = 5.062$ Å, $b = 8.788$ Å, $c = 9.753$ Å, and $\beta = 100.212°$ at 295 K. Figure 1 shows the crystal structure of monoclinic Li_2TiO_3 as reported by Kataoka et al.[34] The agreement with the two sets of experimental data at room temperature is very good with a difference of less than 1.5% for all three lattice dimensions. The good agreement with experimental data gives us confidence in our potential shell model, especially given the fact that the Li_2TiO_3 structure was not used in the derivation of the Li and TiO_2[27,28] potential parameters.

Molecular Dynamics Simulations. MD simulations were carried out with the computer program DL_POLY[32] at 300 K and zero-applied pressure. Trajectories were generated in the NPT ensemble (constant number of particles, constant pressure, and constant temperature), whereby both the cell shape and the size were able to vary. In these simulations, the temperature and pressure were kept constant by use of the Nosé−Hoover thermostat[35] and the Hoover barostat,[36] respectively. The electrostatic forces were calculated by means of the Ewald summation method.[37] A 9 Å cutoff was used for the short-range interactions and the real part of the Ewald sum. The Verlet leapfrog integration algorithm was used to integrate the equations of motion with a time step of 0.2 fs. The shells were given a mass of 0.2 au and their motion treated as that of the cores following the adiabatic shell model first introduced by Mitchell and Fincham.[38]

Nudged Elastic Band (NEB) Calculations. The NEB approach, as implemented in the computer program DL_POLY,[32] was used to generate energy profiles for Li diffusion between lattice sites in Li_2TiO_3. The DL_POLY implementation is based on the method of Henkelman and Jónsson.[39] In the NEB approach, a series of configurations, referred to as "beads", are generated by linear interpolation between a start and an end configuration. Each bead is linked to its nearest neighbors with a harmonic spring with spring constant, k_{NEB}. The system is then optimized to minimize the total energy of the system, that is, including that of the beads. The start and end configurations were each obtained from a conjugate gradients minimization of a $4 \times 3 \times 3$ Li_2TiO_3 supercell with a Li vacancy at the final and initial positions of the diffusing Li ion, respectively. A chain of nine beads with $k_{NEB} = 0.1$ eV Å^{-2} was used throughout. All minimizations were carried out until the forces were converged to 10^{-6} eV Å^{-1}.

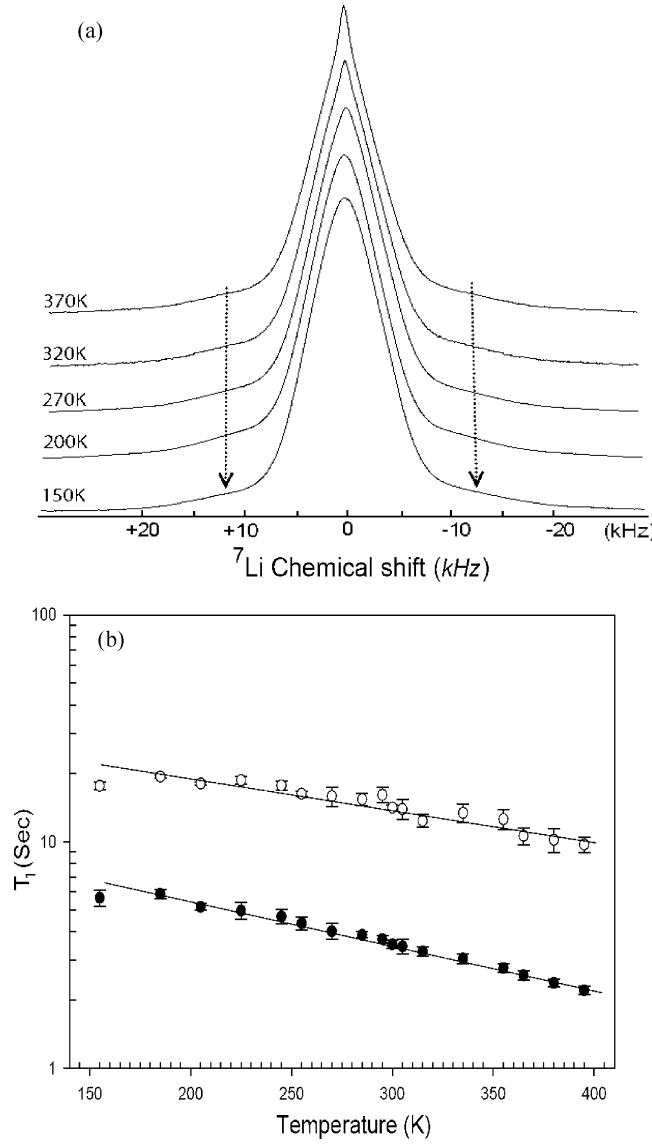

Figure 2. ^{7}Li static NMR spectra measured at a Larmor frequency of 116.53 MHz (7.05 T) for monoclinic Li_2TiO_3. (a) Variable-temperature ^{7}Li static NMR spectra (the arrow indicates the trend of satellite peak position with temperature). (b) Temperature dependence of ^{7}Li spin−lattice relaxation (T_1); lines are to guide the eye.

Results and Discussion

^{7}Li Static NMR. Figure 2a shows the variable-temperature static ^{7}Li NMR spectra of Li_2TiO_3 recorded at 7.05 T magnetic field. The quadrupole satellites in the ^{7}Li spectra show a quadrupolar splitting (ν_Q) of about 24 kHz, which translates into a quadrupolar constant (C_Q) of about 75 kHz, which is a typical value for lithium ion conductors.[15] However, no clear singularities are observed for the quadrupolar satellites; rather, they are smeared out, indicative of disorder in the lithium sublattice due to the distribution of electric field gradients (EFG) at the Li ion sites. The diffusion of lithium ions in solids is through

translational jumps from one discrete site to another rather than via rotational jumps. Therefore, the line narrowing observed in ^{7}Li spectra can be correlated to lithium translational jumps. The lithium translational jumps are known to change the EFG tensor, which can affect satellite transition of ^{7}Li spectra.[15] The satellite patterns in the ^{7}Li NMR spectra in Figure 2 show no significant changes in either shape or width over the whole temperature range (150−400 K). This indicates that no significant amount of lithium translational jumps is taking place in this temperature range. This means most of the lithium ions experience a rigid-lattice regime, that is, $\tau_c\omega_Q > 1$, where τ_c is the correlation time for lithium motion and ω_Q is the quadrupolar frequency. The central transition line width (∼12 kHz) remains constant up to 260 K, and, above this temperature, a partial motional narrowing is observed (see Figure 2a). To gain more insight into the dynamics of lithium diffusion, we performed traditional spin−lattice relaxation (T_1) measurements. Figure 2b shows the temperature dependence of the spin−lattice relaxation measured under a 7 T magnetic field using the inversion recovery method. The magnetization recovery shows biexponential nature indicating at least two different lithium sites in this material. Both T_1 components show monotonous decrease with increasing temperature, indicating a nondiffusive relaxation, which arises mainly from lattice vibrations. This type of relaxation behavior was previously observed in $Li_4Ti_5O_{12}$, in which the lithium jump rates are too slow to affect the spin−lattice relaxation process.[40] Combining these results, we can suggest, with good confidence, that, in the observed temperature range, the lithium jump rates are significantly low and that only a fraction of the lithium ions are taking part in the lithium diffusion process. Because the slow and partial lithium diffusion only has a minimal effect on the observed line width and spin−lattice relaxation, one needs a more quantitative experiment to explore the lithium diffusion characteristics of Li_2TiO_3.

^{7}Li Spin-Alignment Echo NMR. Quadrupolar spin-alignment echo (SAE) NMR is a sensitive and quantitative tool that can probe lithium jump rates in complex ionic conductors.[23,41] Figure 3a shows a set of spin-alignment echoes (S_2) recorded at various temperatures for a fixed preparation time (t_p) of 15 μs. In the low temperature regime ($T < 260$ K), the echo decays are clearly composed of a fast and slow component. The spin-alignment echo decay is generally due to two processes, individual jumps of the spins between electrically nonequivalent crystallographic sites and quadrupolar spin−lattice relaxation (T_{1Q}). The fast component, which reflects the lithium hopping correlation function, can be fitted by a stretched exponential function $(1 - S_0)\exp[-(t_m/\tau_{SAE})^{\beta}]$, where S_0 is the final state correlation value and β is the stretched exponential factor. The second decay component, which arises due to spin−lattice relaxation processes, shows a simple exponential decay behavior. At low temperatures ($T < 260$ K), both processes can be simultaneously measured and well separated from each other. This is due to the fact that they proceed on significantly different time scales. At high temperatures ($T > 260$ K), the SAE decay is dominated by lithium diffusion, and the contribution from spin−lattice relaxation is weak. To extract information on the lithium diffusion only, the slowly decaying component was subtracted from the total echo, and the resulting data set was then fitted with a stretched exponential, which directly yielded the lithium jump rate ($1/\tau_{SAE}$). The stretched exponential factor (β) was found to be on the order of 0.70 ± 0.02. This high β value suggests a narrow distribution of Li jump rates in Li_2TiO_3, which, in turn, indicates that lithium diffusion takes place within a highly ordered structure. The corresponding lithium jump rates

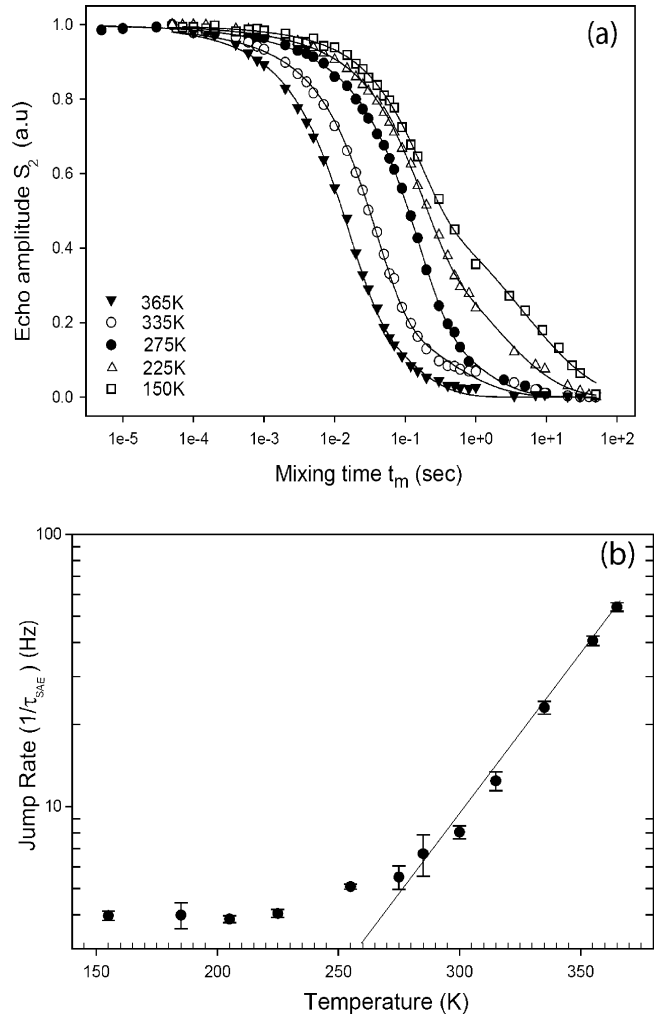

Figure 3. (a) Decay of the ^{7}Li stimulated echo amplitudes (S_2) of Li_2TiO_3 as a function of mixing time (t_m) with preparation time (t_p) as 15 μs at a Larmor frequency of 116.53 MHz. Symbols are experimental points, and lines represent biexponential curve fitting (see text for details). (b) Temperature dependence of lithium jump rate derived from ^{7}Li stimulated echo NMR for Li_2TiO_3; line represents Arrhenius fit, yielding an activation energy of 0.27 ± 0.04 eV.

($1/\tau_{SAE}$) at each temperature are shown in Figure 3b. Lithium diffusion is thermally activated above 260 K, whereas, below this temperature, the lithium jump rate is constant. This result is consistent with the line-narrowing effect observed above 260 K in the variable-temperature ^{7}Li static experiments discussed above. The low temperature regime ($T < 260$ K), often referred to as the rigid-lattice regime, shows the absence of any significant lithium diffusion. In this regime, the SAE decay is primarily induced by other effects of nondiffusive nature such as ordinary spin−lattice relaxation or spin-diffusion (i.e., spin flip-flop). Considering the temperature independence of the jump rate, we can conclude that the SAE decay is dominated by spin-diffusion in the low temperature regime. The onset of lithium diffusion at 260 K leads to activated lithium dynamics, which will be referred to as the "high temperature regime". Even in the high temperature regime, lithium jump rates are extremely slow. For example, the lithium jump rate is only 60 Hz at 350 K, which is relatively low compared to other lithium ionic conductors reported in literature.[23,42,43] This slow lithium diffusion behavior might explain the low conductivity reported for this material.[13] In the high temperature regime, the lithium jump rate ($1/\tau_{SAE}$) follows an Arrhenius behavior with activation

energy of 0.27 ± 0.04 eV. The fact that lithium diffusion is very slow despite a relatively low energy barrier can be explained by the fact that successive lithium jumps require the presence of lithium vacancies in the crystal lattice. In fully stoichiometric Li_2TiO_3, all of the regular lithium positions are occupied, and interstitial positions such as the tetrahedral position are not favorable due to the high repulsive force between neighboring Li ions. However, nonstoichiometric Li_2TiO_3 can have lithium vacancies, thereby making lithium diffusion possible. Such nonstoichiometric type Li_2TiO_3 samples, synthesized by various methods, have been previously reported in the literature.[12,44,45] Hence, the hydrothermally prepared Li_2TiO_3 sample might show a slight deviation from stoichiometry, which in turn can provide suitable vacancies for lithium jumps. With ^{7}Li SAE NMR, only those Li jumps that lead to changes in the corresponding quadrupole frequencies (ω_Q) can be detected. Therefore, jumps between equivalent lithium sites are not "seen" by SAE NMR because no change of the quadrupole frequency occurs.[23] Hence, the observed lithium diffusion in SAE must represent lithium hopping between different crystallographic sites in Li_2TiO_3. Even though ^{7}Li SAE NMR provides direct measurement of the lithium jump rates, it lacks information about possible lithium diffusion pathways. A more elaborated view of lithium dynamics requires the spectral resolution of individual lithium sites. This can be achieved by employing ^{6}Li MAS NMR under high magnetic field.

^{6}Li MAS NMR. The low gyromagnetic ratio of ^{6}Li nucleus in combination with its low natural abundance (about 7%) and quadrupole moment (-8×10^{24} Q/m^2) entail weaker homonuclear dipole−dipole interactions and quadrupolar broadening.[46] Hence, ^{6}Li NMR combined with MAS and high magnetic field can offer a better spectral resolution than traditional ^{7}Li MAS NMR. Figure 4a shows the observed and deconvoluted ^{6}Li MAS NMR spectra of Li_2TiO_3 recorded at 300 and 470 K under 21.1 T with a spinning speed of 7 kHz. The room-temperature (300 K) ^{6}Li MAS NMR spectra show three resonances at −0.80, −0.22, and 0.24 ppm, which are labeled as A, B, and C, respectively (see Figure 4a), and are indicative of three different environments for lithium in the hydrothermally prepared Li_2TiO_3 sample. According to lithium chemical shift correlation data,[47,48] the peaks at −0.80 and −0.22 ppm (peaks A and B) should be assigned to lithium ions in octahedral sites (LiO_6) and the small peak at 0.24 ppm (peak C) to lithium in tetrahedral coordination (LiO_4). These ^{6}Li peak assignments for different lithium positions are in good agreement with previous reports on lithium inserted titanium oxide materials.[49−52] However, the single crystal structure[53] of Li_2TiO_3 indicates that all three lithium sites (labeled as Li1, Li2, and Li3) have an octahedral coordination, as shown in Figure 1. As we discussed earlier, the hydrothermally prepared Li_2TiO_3 sample might have slight deviation from stoichiometry, which could result in the presence of lithium vacancies, which, in turn, could make new sites, including tetrahedral sites, available to lithium ions. This hypothesis is verified in the next section using atomistic simulation techniques, which reveal the availability of lithium tetrahedral sites in slightly Li-deficient/Ti-rich Li_2TiO_3 samples. Combining these results, peak C can be assigned to lithium in a new tetrahedral position. The remaining two peaks, A and B, are assigned on the basis of the Li_2TiO_3 crystal structure. The lithium sites Li1 and Li2, which are positioned in the pure Li layer, have very similar nearest-neighbor distances[53] and are therefore expected to exhibit very similar chemical shifts in the ^{6}Li NMR spectra. Furthermore, the lithium ions in sites Li1 and Li2 constitute 50% and 25%, respectively, of the total number of lithium ions in the Li_2TiO_3 structure, whereby the remaining 25% are found in the Li3 sites in the $LiTi_2$ layer.[54] In general, the ratio of the integrated signal of the three resonances equals the ratio of the amount of lithium in the respective environments. Hence, peak A, which represents approximately 70% of the total integral intensity, can be assigned to lithium ions in the Li1 and Li2 sites. The integral intensity of peak B is approximately 20% and can be assigned to lithium ions located in the Li3 position. The relatively higher chemical shielding at this site can be explained by the fact that the LiO_6 polyhedron shares faces with TiO_6 octahedra rather than with LiO_6 octahedra for the Li1 and Li2 sites (see Figure 1). This results in smaller Li−O bond length for Li3 site than the Li1 and Li2 sites, resulting in more shielding and hence peak shift toward positive chemical shift value. Having assigned all three peaks, the ^{6}Li MAS NMR spectra can offer further information on the possible lithium diffusion pathways in Li_2TiO_3 by studying the temperature dependence of the peak positions. Indeed, lithium hopping between two different sites

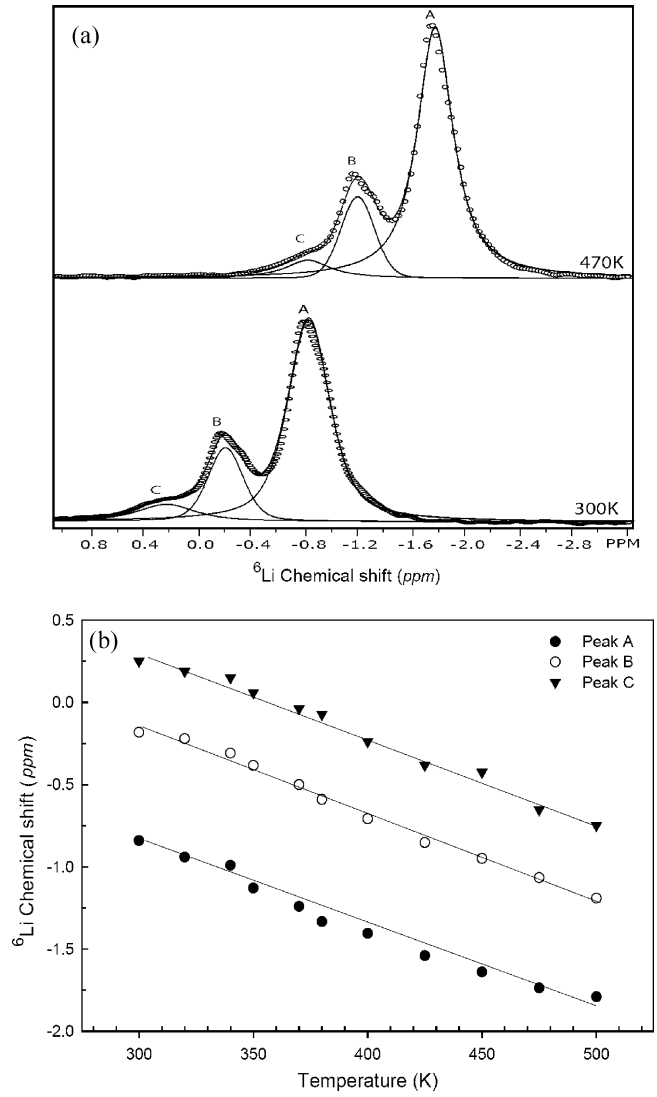

Figure 4. ^{6}Li MAS NMR spectra measured at 21.1 T with spinning frequency of 10 kHz of the three resonance peaks. (a) Deconvoluted variable-temperature ^{6}Li MAS NMR spectra at 300 K (bottom) and 470 K (top), with dotted lines and solid lines representing the experimental spectrum and fitted Gaussian/Lorentizan line shape, respectively. (b) Temperature dependence of ^{6}Li isotropic chemical shift for monoclinic Li_2TiO_3; lines are to guide the eye.

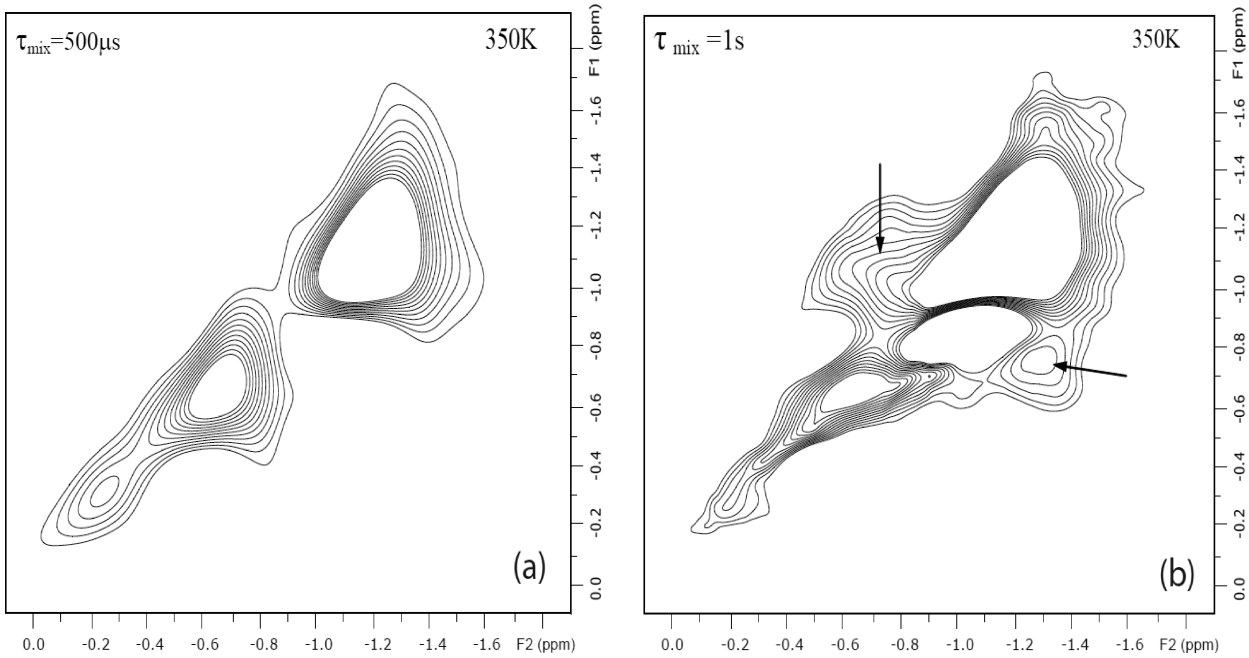

Figure 5. ^{6}Li −2D exchange spectra measured at 21.1 T with a spinning frequency of 10 kHz for monoclinic Li_2TiO_3 with $T = 350$ K and mixing time $\tau_{mix} = 500$ μs (a) and $\tau_{mix} = 1$ s (b). The cross peaks observed for mixing time $\tau_{mix} = 1$ s (b) are indicated by the arrow marks.

leads to the coalescence of ^{6}Li resonance peaks. The main characteristic feature of coalescence is the change of isotropic chemical shift observed when two peaks, representing two different chemical sites, move toward each other. Figure 4b shows the temperature dependence of the chemical shift of all three lithium resonances. As can be seen from Figure 4b, there is no significant change in the isotropic chemical shift between any of the three lithium resonances in the temperature range considered in this study (300−500 K). All three lithium resonances monotonously shift toward negative chemical shifts with increasing temperature without any indication of collapse or merging of peaks. This reveals that there is no significant lithium hopping between the different sites, an observation that is consistent with the ^{7}Li static spectra discussed earlier. However, there are small changes (within the error limitations, i.e., ±5%) in the integral intensity of the peaks with increasing temperature, which suggests the possibility of a small fraction of lithium engaged in hopping between different lithium sites. This hypothesis can be validated by employing two-dimensional ^{6}Li exchange spectroscopy, which offers direct evidence for lithium hopping between nonequivalent sites.[25]

In 2D exchange spectroscopy, the frequency $\omega(t_1)$ of a given lithium ion at time t_1 is correlated with the frequency $\omega(t_2)$ after a mixing time τ_{mix}. If no jump occurs during the mixing time, then $\omega(t_1) = \omega(t_2)$, and only diagonal peaks appear in the 2D spectrum. On the other hand, if lithium jumps to a different position during the mixing time, then $\omega(t_1) \neq \omega(t_2)$, resulting in the presence of peaks at off-diagonal positions along with regular diagonal peaks. The off-diagonal peaks directly relate to the jump between different lithium sites. Figures 5a and 5b show ^{6}Li 2D-exchange MAS NMR spectra measured at 350 K under a 21.1 T magnetic field with mixing times of $\tau_{mix} = 500$ μs and $\tau_{mix} = 1$ s, respectively. As is clearly seen in Figure 5a, for a mixing time of 500 μs only diagonal peaks are observed, indicating that no lithium jump occurs during this mixing time, whereas for a mixing time of 1 s, lithium jumps are evidenced by the presence of significant off-diagonal intensity. In fact, the off-diagonal peaks (marked by the two black arrows in Figure 5b) at −1 ppm in the F1 dimension and −0.7 ppm in the F2 dimension are a clear indication of lithium jumps between the Li_3 (sites Li1 and Li2) and $LiTi_2$ layers (sites Li3) along the *c* axis. There are no visible cross peaks involving the tetrahedral lithium site (i.e., peak C); however, considering the small intensity of peak C, any cross peaks arising from peak C will be much smaller and will likely be buried under the noise. This means that, even though there are no observed diagonal peaks involving peak C, lithium jumps between the tetrahedral position and other lithium sites (Li1, Li2, or Li3) cannot be ruled out. To examine the potential requirement for these lithium diffusion pathways, we carried out an extensive molecular dynamics study of lithium diffusion in this material.

Atomistic Simulation of Li Diffusion. A $4 \times 3 \times 3$ Li_2TiO_3 supercell was generated to study Li diffusion between the different Li sites in Li_2TiO_3. In the Li_2TiO_3 lattice, all of the Li ions occupy octahedral sites, and, although tetrahedral sites are formed by the oxygen sublattice, they are empty, mainly due to the Li−Li repulsion that would result from a Li ion moving from an octahedral to a tetrahedral site. We first set out to evaluate whether the lithium ions occupied more than one position in their respective octahedral sites, as it has been shown to be the case for lithium in the octahedral sites of lithiated anatase and lithium titanate.[55] The Li atomic density along the normal to the *ab* plane was obtained from a molecular dynamics simulation at 300 K. Each peak was successfully fitted using a single Gaussian distribution, indicating that all three Li ions occupy a single position in the *c* direction. The atomic density distributions thus obtained are shown in Figure 6. The average variance of each density distribution shows that the vibrational amplitude in the *c* direction follows the order: Li3 > Li2 > Li1. This initial MD simulation suggests that we only need to consider one position per crystallographic site in our calculations of the Li energy profiles. Therefore, the energy profile for Li diffusion from Li_A to Li_B, where A and B each corresponds to one of the three crystallographic sites, was obtained by creating a vacancy at the Li_B site and moving a Li ion at the Li_A site to the vacant Li_B site using the NEB approach. Only Li−Li nearest-neighbor jumps were considered. Several nearest-neighbor jumps are possible for each of the three crystallographic sites. Using

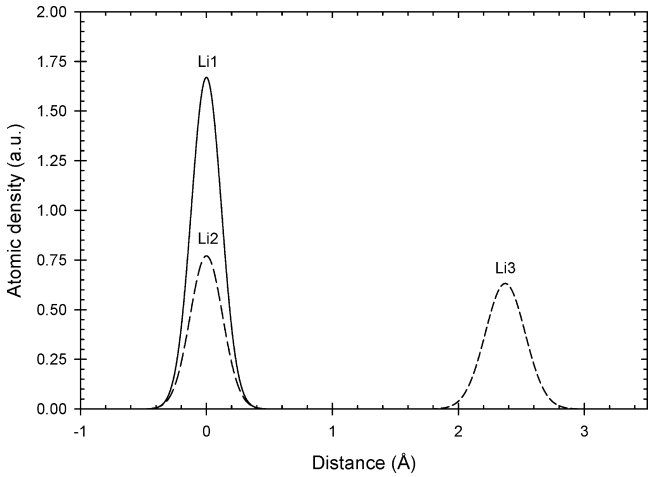

Figure 6. Li atomic density of monoclinic Li_2TiO_3 (along the *c* direction) at 300 K, calculated using molecular dynamics simulation. The position of the peaks was normalized to the average height of the Li1 site at pure Li layer.

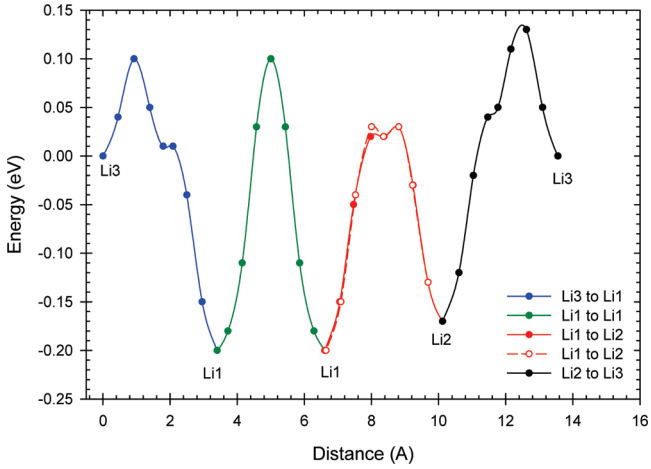

Figure 7. Energy profiles for Li jumps between three Li crystallographic sites in monoclinic Li_2TiO_3 lattice obtained from nudged elastic band calculations.

the relaxed structure obtained with the potential model, we determined that there are, from Li1, three jumps to a Li1 site with jump distances of 2.63 (2.79), 3.08 (3.00), and 3.10 (3.00) Å and three jumps to a Li2 site with jump distances of 2.86 (2.89), 2.86 (2.90), and 3.10 (2.99) Å. (The distances in brackets are those obtained with the XRD data of Kataoka et al.[34] for the same jump.) From Li2, there are three sets of two equivalent jumps to a Li1 site with jump distances of 2.86 (2.89), 2.86 (2.90), and 3.08 (2.99) Å. Finally, there are four Li1 sites accessible from Li3 at 2.81 (2.91) Å and two Li2 sites at 2.88 (2.92) Å. The energy profiles of all jumps just described were calculated with the NEB approach; however, Figure 7 only shows the energy profile of the following jumps: 2.63(2.79) Å Li1−Li1, 2.86(2.89) Å Li1−Li2, 2.86(2.90) Å Li1−Li2, 2.81(2.91) Å Li3−Li1, and 2.88(2.91) Å Li3−Li2. The remaining jumps are not shown as they resulted in a much higher activation energy of 0.75 eV or greater and are therefore unlikely to play a significant role in the overall Li diffusion. Several important findings emerged from Figure 7. First, the three Li sites are not energetically equivalent. There is a large energy gain from moving a Li3 ion to a neighboring vacant Li1 site (0.17 eV) and a smaller energy gain between the Li1 and Li2 sites (0.03 eV). This result suggests that, in an otherwise perfect lattice, a Li vacancy will preferably reside in the $LiTi_2$ layer.

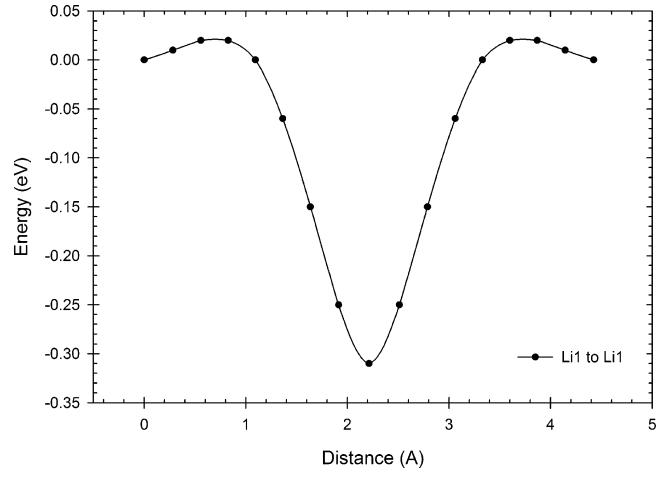

Figure 8. Energy profile for a Li1 to Li1 jump along the *ab* plane, in the presence of a Li vacancy in the $LiTi_2$ layer of monoclinic Li_2TiO_3 lattice, calculated using the nudged elastic band method.

Second, the activation energies are in agreement with the effective activation energy of 0.27 ± 0.04 eV obtained in the present NMR experiments (Li1 to Li1, 0.30 (0.30) eV; Li1 to Li2, 0.20 (0.23) eV; Li1 to Li3, 0.30 (0.10) eV; and Li2 to Li3, 0.30 (0.13) eV with the backward activation energy shown in brackets). Finally, all of the energy profiles shown in Figure 7, except for the Li1 to Li1 jump, show either an inflection point or a very shallow minimum at approximately the midway point of the beads chain. These special points correspond to the diffusing Li ion occupying a tetrahedral site; however, due to the Li−Li repulsion, these configurations are not stable. Therefore, the presence of a Li vacancy is not sufficient to reduce the Li−Li repulsion and make the tetrahedral site accessible. Interestingly, if a Li vacancy is created in the nearest Li3 site and the Li1 to Li1 NEB calculation is repeated (the number of beads was doubled), a new minimum appears that is 0.31 eV more stable than the configuration where the Li vacancies occupy the Li1 and Li3 sites (shown in Figure 8). In this configuration, the diffusing Li ion and a second Li ion, which was displaced from a Li3 site, occupy a tetrahedral site. The two Li ions are symmetrically equivalent with Li−O distances of 1.91, 1.94, 1.94, and 1.99 Å. These calculations therefore show that the tetrahedral site will be readily occupied when two Li vacancies are in proximity (note the very low activation energy for hopping to the tetrahedral site in this situation, Figure 8).

Finally, the samples used in this study showed a slight deviation from stoichiometry as has been observed in previous studies of this material.[12,44,45] Therefore, we investigated the effects of substituting a Ti atom for a Li atom in the $LiTi_2$ layer (i.e., at the Li3 site). An energy minimization of the 4 × 3 × 3 Li_2TiO_3 supercell used previously with a Li3 replaced by a Ti^{4+} ion was carried out with the conjugate gradients technique. The extra Ti ion remained in a 6-fold coordination with Ti−O bond distances of 1.957 Å (×2), 1.960 Å (×2), and 1.970 Å (×2). These distances are similar to those of the two Ti crystallographic positions Ti1 (1.956 Å (×2), 1.962 Å (×2), and 1.964 Å (×2)) and Ti2 (1.957 Å (×4) and 1.962 Å (×2)) and differ significantly from those of the Li3 site (2.085 Å (×2), 2.088 Å (×2), and 2.097 Å (×2)). Next, we investigated the charge neutralization of the Ti substitution defect by three Li vacancies. A series of configurations in which the three Li vacancies arrange between nearest-neighbor Li sites was considered. If only considering nearest-neighbor Li sites, the

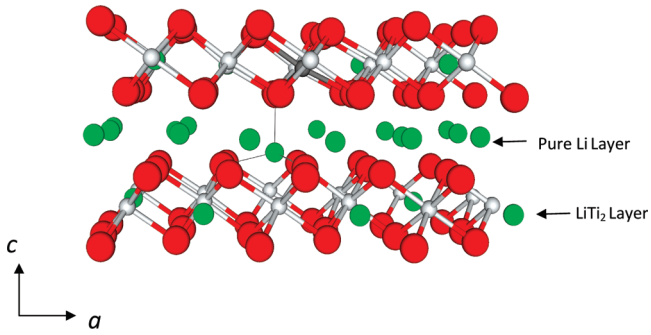

Figure 9. The tetrahedral site occupied by Li ion (with solid lines showing coordination to nearest-neighbor oxygen ions) in the presence of a Ti substitution at the Li3 site along with charge-neutralizing Li vacancies in the *ab* plane of monoclinic Li_2TiO_3. Lithium atoms are shown in light and dark green, oxygen atoms in red, and titanium atoms in gray with the additional Ti atom shown in dark gray.

vacancies can distribute between 4 Li1, 2 Li2, and 6 Li3 sites. The energy of 12 such configurations was calculated. All of the configurations are fairly close in energy and span approximately 0.12 eV. The least energetically favored configurations include those where the three Li vacancies are located at Li3 sites or where two are at Li3 sites and one is at a Li2 site. The most energetically favored include configurations where the vacancies are located at three Li1 sites, two Li1 and one Li2 site, or two Li1 and one Li3 site. We considered two additional configurations. In the Li_2TiO_3 structure, the tetrahedral site has a Li ion near three of its faces in the *ab* plane and one Li or Ti atom near its fourth face along the *c* direction. In the two additional configurations, three Li ions that surround one tetrahedral site in the *ab* plane were removed, and the fourth Li ion was moved from the Li3 site to the tetrahedral site. Two configurations are possible depending on whether one or two of the three Li ions removed from the *ab* plane are nearest neighbors of the Ti defect. The configuration where two of the three Li removed are nearest neighbors of the Ti defect was calculated to be the most energetically stable of all configurations considered and 0.04 eV more stable than the next most energetically favored configurations described above. A schematic of this configuration is shown in Figure 9. Therefore, our potential model calculations strongly suggest that Li ions in 4-fold coordination can be found as a result of the formation of a Ti-rich $TiLi_2$ layer.

Li Diffusion Mechanism in Li_2TiO_3. By combining both the NMR and the MD simulation results, we can draw a clear picture of the possible lithium diffusion mechanisms in monoclinic Li_2TiO_3. In the presence of vacancies, two directions for lithium diffusion are possible in Li_2TiO_3, lithium diffusion along the *ab* plane (i.e., lithium jumps among Li1 and Li2 sites in the pure Li layer) and along the *c* axis (i.e., lithium jumps between Li1/Li2 and Li3 sites between the pure Li and $LiTi_2$ layers).

For lithium diffusion along the *ab* plane, it is essential to have lithium vacancies at either the Li1 or the Li2 sites. Our MD calculations show that an isolated Li vacancy will preferably reside in the Li3 site, whereas in the presence of a Ti defect in the $LiTi_2$ layer, Li vacancies will preferably migrate to Li1 and Li2 sites and will allow for the displacement of a Li3 ion to the tetrahedral site. The detection of ^{6}Li resonance (peak C in Figure 4a) corresponding to lithium in a tetrahedral position suggests the presence of vacancies in Li1 and Li2 sites in the pure Li layer. With the presence of lithium vacancies in Li1/Li2 sites, the diffusion along the *ab* plane becomes possible. Figure 10a shows a possible pathway for lithium diffusion from Li1 to Li2 along the *ab* plane predicted from NEB calculations. The

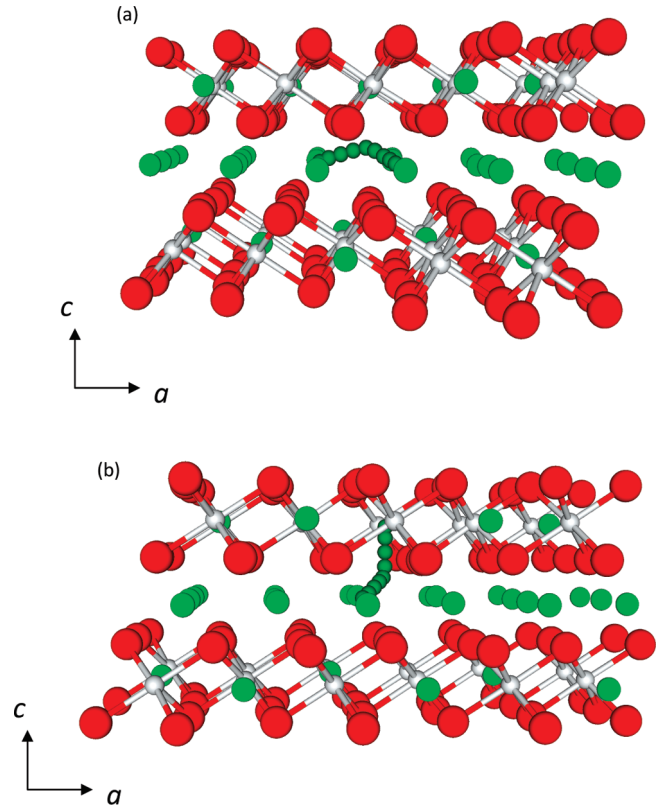

Figure 10. Example of lithium jump pathways in monoclinic Li_2TiO_3 (viewed along the *b* axis) predicted with the nudged elastic band approach: (a) lithium diffusion along the *ab* plane for the Li1−Li2 jump; and (b) lithium diffusion along the *c* axis for the Li1−Li3 jump.

activation energy for lithium hopping between Li1 and Li2 sites is relatively low (0.20 eV) as compared to that between two Li1 sites (0.30 eV). This activation energy is in good agreement with the activation energy derived from the ^{7}Li SAE measurement. However, there is no direct evidence for lithium diffusion along the *ab* plane in our NMR studies. This is mainly due to the lack of ^{6}Li chemical shift resolution between the Li1 and Li2 sites in the pure Li layer. Hence, there might be lithium diffusion along the *ab* plane due to lithium vacancies in the pure Li layer.

Lithium diffusion along the *c* axis is initially considered as energetically costly due to the high repulsive force expected from Ti cations in $LiTi_2$ layer. Yet our MD simulation shows that the lithium jumps between Li1/Li2 and Li3 sites along the *c* axis have a similar activation energy (0.30 eV) as that for lithium diffusion along the *ab* plane and are in good agreement with the activation energy derived from ^{7}Li SAE NMR. Figure 10b shows a possible pathway for lithium diffusion along the *c* axis as determined from NEB calculations. Furthermore, the cross peaks observed in the 2D ^{6}Li exchange spectra (see Figure 5) give direct evidence for lithium diffusion between Li1/Li2 and Li3 sites. Overall, the lithium diffusion along both the *ab* plane and the *c* axis is limited by the availability of vacancies, and the formation of vacancies depends on lithium stoichiometry in Li_2TiO_3.

Conclusions

This study clearly demonstrates the advantages of combining ^{6,7}Li NMR and MD simulations to explore the ion dynamics in ceramic materials. The variable-temperature ^{7}Li static NMR shows partial line narrowing at about 260 K, indicating the onset

of lithium diffusion albeit with only a fraction of lithium actively participating in the diffusion process. The lithium jump rate determined using ^{7}Li stimulated echo experiments is very slow, that is, 60 Hz at 350 K. This partial and slow lithium diffusion process is limited by the availability of nearby vacancies. The hydrothermally prepared Li_2TiO_3 has a slight deviation in lithium stoichiometry, which, in turn, causes additional vacancies in the monoclinic structure. Our MD calculations show that an isolated Li vacancy will preferably reside in the Li3 site, but in the presence of a Ti defect in the $LiTi_2$ layer, Li vacancies will preferably migrate to the Li1 and Li2 sites and will allow for the displacement of a Li3 ion to the tetrahedral site. Although this tetrahedral site is available in stoichiometric Li_2TiO_3, it is occupied by lithium only when two or more Li vacancies are formed due to Ti defects in $LiTi_2$ layer. This new tetrahedral lithium occupation has been detected, along with the three crystallographic octahedral lithium sites, in the hydrothermally prepared nonstoichiometric Li_2TiO_3 sample using high-field ^{6}Li MAS NMR. The variable-temperature ^{6}Li MAS NMR shows that there is no significant lithium diffusion in the temperature range between 300 and 500 K. The lithium diffusion pathways were obtained employing ^{6}Li 2D exchange NMR, which clearly indicates that lithium diffusion takes place between Li1/Li2 and Li3 sites along the *c* axis. In addition, our MD simulations show lithium diffusion in the pure Li layer along the *ab* plane is equally probable provided nearby vacancies are available. Considering the fact that a nonstoichiometric Li_2TiO_3 can cause lithium vacancies in both the pure Li and the $LiTi_2$ layers, lithium diffusion should take place along the *c* axis and in the *ab* plane. This means lithium conduction in monoclinic Li_2TiO_3 is three-dimensional provided suitable nearby vacancies are available. However, the lithium jump rate between any sites is extremely slow (60 Hz at 350 K) as compared to other traditional lithium ionic conductors. Hence, the poor conductivity reported in monoclinic Li_2TiO_3 between 300 and 500 K can be explained by the slow and partial lithium diffusion behavior of this material.

Acknowledgment. This work is supported by the Laboratory-Directed Research and Development Program (LDRD) of the Pacific Northwest National Laboratory (PNNL) and by the Office of Basic Energy Sciences (BES), U.S. Department of Energy (DOE). The NMR work was carried out at the Environmental and Molecular Science Laboratory, a national scientific user facility sponsored by the DOE's Office of Biological and Environmental Research (BER). PNNL is a multiprogram laboratory operated by Battelle Memorial Institute for the Department of Energy under contract DE-AC05-76RL01830.

References and Notes

(1) Zhang, L.; Wang, X.; Noguchi, H.; Yoshio, M.; Takada, K.; Sasaki, T. *Electrochim. Acta* **2004**, *49*, 3305.
(2) Johnson, C. S.; Kim, J.-S.; Kropf, A. J.; Kahaian, A. J.; Vaughey, J. T.; Thackeray, M. M. *J. Power Sources* **2003**, *119−121*, 139.
(3) Chauvaut, V.; Cassir, M. *J. Electroanal. Chem.* **1999**, *474*, 9.
(4) Roux, N.; Avon, J.; Floreancing, A.; Mougin, J.; Rasneur, B.; Ravel, S. *J. Nucl. Mater.* **1996**, *233−237*, 1431.
(5) Shigemura, H.; Tabuchi, M.; Sakaebe, H.; Kobayashi, H.; Kageyama, H. *J. Electrochem. Soc.* **2003**, *150*, A638.
(6) Kim, J. S.; Johnson, C. S.; Thackeray, M. M. *Electrochem. Commun.* **2002**, *4*, 205.
(7) Zhang, L.; Muta, T.; Noguchi, H.; Wang, X.; Zhou, M.; Yoshio, M. *J. Power Sources* **2003**, *117*, 137.
(8) Zhang, L.; Noguchi, H. *J. Electrochem. Soc.* **2003**, *150*, A601.
(9) Hashimoto, K.; Nishikawa, M.; Nakashima, N.; Beloglazov, S.; Enoeda, M. *Fusion Eng. Des.* **2002**, *61−62*, 375.
(10) Gierszewski, P. *Fusion Eng. Des.* **1998**, *39−40*, 739.
(11) Saito, S.; Tsuchiya, K.; Kawamura, H.; Terai, T.; Tanaka, S. *J. Nucl. Mater.* **1998**, *253*, 213.
(12) Kleykamp, H. *Fusion Eng. Des.* **2002**, *61−62*, 361.
(13) Fehr, T.; Schmidbauer, E. *Solid State Ionics* **2007**, *178*, 35.
(14) Vītiņš, Ģ. V.; Ķizāne, G.; Lūsis, A.; Tīliks, J. *J. Solid State Electrochem.* **2002**, *6*, 311.
(15) Böhmer, R.; Jeffrey, K. R.; Vogel, M. *Prog. Nucl. Magn. Reson. Spectrosc.* **2007**, *50*, 87.
(16) Vijayakumar, M.; Emery, J.; Bohnke, O.; Vold, R. L.; Hoatson, G. L. *Solid State Ionics* **2006**, *177*, 1673.
(17) Bain, A. D. *Prog. Nucl. Magn. Reson. Spectrosc.* **2003**, *43*, 63.
(18) Wilkening, M.; Heitjans, P. *Solid State Ionics* **2006**, *177*, 3031.
(19) Tomiha, M.; Masaki, N.; Uchida, S.; Sato, T. *J. Mater. Sci.* **2002**, *37*, 2341.
(20) Jeener, J.; Broekaert, P. *Phys. Rev.* **1967**, *157*, 232.
(21) Böhmer, R. *J. Magn. Reson.* **2000**, *147*, 78.
(22) Böhmer, R.; Jörg, T.; Qi, F.; Titze, A. *Chem. Phys. Lett.* **2000**, *316*, 419.
(23) Wilkening, M.; Heitjans, P. *Phys. Rev. B: Condens. Matter Mater. Phys.* **2008**, *77*, 024311.
(24) Massiot, D. F. F.; Capron, M.; King, I.; Le Calvé, S.; Alonso, B.; Durand, J.-O.; Bujoli, B.; Gan, Z.; Hoatson, G. *Magn. Reson. Chem.* **2002**, *40*, 70.
(25) Jeener, J.; Meier, B. H.; Bachmann, P.; Ernst, R. R. *J. Chem. Phys.* **1979**, *71*, 4546.
(26) Born, M.; Huang, K. *Dynamical Theory of Crystal Lattices*; Oxford University Press: Oxford, UK, 1954.
(27) Matsui, M.; Akaogi, M. *Mol. Simul.* **1991**, *6*, 239.
(28) Kerisit, S.; Deskins, N. A.; Rosso, K. M.; Dupuis, M. *J. Phys. Chem. C* **2008**, *112*, 7678.
(29) Deskins, N. A.; Dupuis, M. *Phys. Rev. B* **2007**, *75*, 195212.
(30) Dick, B. G.; Overhauser, A. W. *Phys. Rev.* **1958**, *112*, 90.
(31) Watson, G. W.; Kelsey, E. T.; de Leeuw, N. H.; Harris, D. J.; Parker, S. C. *J. Chem. Soc., Faraday Trans.* **1996**, *92*, 433.
(32) Smith, W.; Forester, T. R.; Todorov, I. T. *The DL_POLY_2 User Manual*; Daresbury Laboratory: United Kingdom, 2009.
(33) Dorrian, J. F.; Newnham, R. E. *Mater. Res. Bull.* **1969**, *4*, 179.
(34) Kataoka, K.; Takahashi, Y.; Kijima, N.; Nagai, H.; Akimoto, J.; Idemoto, Y.; Ohshima, K.-I. *Mater. Res. Bull.* **2009**, *44*, 168.
(35) Hoover, W. G. *Phys. Rev. A* **1985**, *31*, 1695.
(36) Melchionna, S.; Ciccotti, G.; Holian, B. L. *Mol. Phys.* **1993**, *78*, 533.
(37) Ewald, P. P. *Ann. Phys.* **1921**, *64*, 253.
(38) Mitchell, P. J.; Fincham, D. *J. Phys.: Condens. Matter* **1993**, *5*, 1031.
(39) Henkelman, G.; Jónsson, H. *J. Chem. Phys.* **2000**, *113*, 9978.
(40) Wilkening, M.; Amade, R.; Iwaniak, W.; Heitjans, P. *Phys. Chem. Chem. Phys.* **2007**, *9*, 1239.
(41) Wilkening, M.; Heitjans, P. *J. Phys.: Condens. Matter* **2006**, *18*, 9849.
(42) Wilkening, M.; Lyness, C.; Armstrong, A. R.; Bruce, P. G. *J. Phys. Chem. C* **2009**, *113*, 4741.
(43) Wilkening, M.; Bork, D.; Indris, S.; Heitjans, P. *Phys. Chem. Chem. Phys.* **2002**, *4*, 3246.
(44) Vītiņš, Ģ.; Ķizāne, G.; Lūsis, A.; Tīliks, J. *J. Solid State Electrochem.* **2002**, *6*, 311.
(45) Hoshino, T.; Dokiya, M.; Terai, T.; Takahashi, Y.; Yamawaki, M. *Fusion Eng. Des.* **2002**, *61−62*, 353.
(46) Bond, S. P. A. G.; Homer, J.; McWhinnie, W. R.; Perry, M. C. *J. Mater. Chem.* **1991**, *1*, 327.
(47) Alam, T. M.; Conzone, S.; Brow, R. K.; Boyle, T. J. *J. Non-Cryst. Solids* **1999**, *258*, 140.
(48) Xu, Z.; Stebbins, J. F. *Solid State Nucl. Magn. Reson.* **1995**, *5*, 103.
(49) Vijayakumar, M.; Kerisit, S.; Wang, C.; Nie, Z.; Rosso, K. M.; Yang, Z.; Graff, G.; Liu, J.; Hu, J. *J. Phys. Chem. C* **2009**, *113*, 14567.
(50) Krtil, P.; Dedecek, J.; Kostlanova, T.; Brus, J. *Electrochem. Solid-State Lett.* **2004**, *7*, A163.
(51) Kostlánová, T.; Dedecek, J.; Krtil, P. *Electrochim. Acta* **2007**, *52*, 1847.
(52) Kartha, J. P.; Tunstall, D. P.; Irvine, J. T. S. *J. Solid State Chem.* **2000**, *152*, 397.
(53) Kataoka, K.; Takahashi, Y.; Kijima, N.; Nagai, H.; Akimoto, J.; Idemoto, Y.; Ohshima, K.-i. *Mater. Res. Bull.* **2009**, *44*, 168.
(54) Zainullina, V. M.; Denisova, V. P. Z. T. A.; Maksimova, L. G. *Zh. Strukt. Khim.* **2003**, *44*, 180.
(55) Wagemaker, M.; Kearley, G. J.; van Well, A. A.; Mutka, H.; Mulder, F. M. *J. Am. Chem. Soc.* **2003**, *125*, 840.

JP9072125